

Image charge detection statistics relevant for deterministic ion implantation

Paul Räche^{1,2,3} , Robert Staacke¹, Jürgen W Gerlach^{2,3}, Jan Meijer^{1,3} and Daniel Spemann^{2,3}

¹ Felix Bloch Institute for Solid State Physics, Universität Leipzig, Linnéstr. 5, 04103 Leipzig, Germany

² Leibniz Institute of Surface Engineering, Permoserstr. 15, 04318 Leipzig, Germany

³ Leibniz Joint Lab ‘Single Ion Implantation’, Permoserstr. 15, 04318 Leipzig, Germany

E-mail: paul.raecke@iom-leipzig.de

Received 4 March 2019, revised 11 April 2019

Accepted for publication 26 April 2019


Published 23 May 2019



Abstract

Image charge detection is a non-perturbative pre-detection approach for deterministic ion implantation. Using low energy ion bunches as a model system for highly charged single ions, we experimentally studied the error and detection rates of an image charge detector setup. The probability density functions of the signal amplitudes in the Fourier spectrum can be modelled with a generalised gamma distribution to predict error and detection rates. It is shown that the false positive error rate can be minimised at the cost of detection rate, but this does not impair the fidelity of a deterministic implantation process. Independent of the ion species, at a signal-to-noise ratio of 2, a false positive error rate of 0.1% is achieved, while the detection rate is about 22%.

Keywords: image charge detection, ion implantation, deterministic implantation, binary detection


 Supplementary material for this article is available [online](#)

(Some figures may appear in colour only in the online journal)

1. Introduction

Image charge detection (ICD) is a technique that can be used to non-perturbatively measure the velocity, charge, mass and other properties of moving charged particles. One example is the mass spectrometry of highly charged, large molecules [1, 2]. The principle is based on the fact that a moving charge induces a moving image charge, i.e. a current signal, in a nearby conductor, as described by the Shockley–Ramo theorem [3, 4].

Our work focusses on the application of ICD for ion implantation. For quantum technologies, the deterministic implantation of low fluences and especially single ions into solid state material is an ongoing challenge [5–7].

 Original content from this work may be used under the terms of the [Creative Commons Attribution 3.0 licence](#). Any further distribution of this work must maintain attribution to the author(s) and the title of the work, journal citation and DOI.

The concept for a deterministic single ion implanter based on ICD and details of the experimental setup used in this study were previously published elsewhere [8]. Even with the most advanced electronic amplifier technology available, an image charge detector for a small number of elementary charges operates at a very low signal-to-noise ratio (SNR), especially when the ion has to be detected in a single pass through the detector, as is required for high-precision ion implantation. In this work, we investigate how the detection and error rates of an image charge detector depend on the SNR. As an image charge detector that provides single ion sensitivity employing a single pass of the ion only, is not yet available, we study the detection of single passes of ion bunches through our detector prototype instead. In this case, the SNR is proportional to the number of ions per bunch. Nevertheless, the main motivation for this work is to transfer the principles to future image charge detectors, that will exhibit less electronic noise, making detection of single ions possible.

Methods for deterministic ion implantation are either based on pre-detection or post-detection approaches. Pre-detection means that the ions are detected before arriving at the sample, including deterministic ion source concepts [9]. For post-detection, secondary signals from the impact and the stopping of the ions in the sample are used. This includes the collection of secondary electrons [10] or the electron–hole pairs from ionisation in the substrate (ion beam induced charge (IBIC)) [5, 6]. ICD is a pre-detection method. Only in case of a successful detection, the incoming ion is allowed to be implanted. In case of an unclear signal in the detector, the ion is rejected by means of a beam blarker downstream. Thus, the sample remains unchanged. Even if ions pass the detector unnoticed, the fidelity of the implantation is unaffected, only the implantation rate is lowered. The detection error that has to be reduced as much as possible is the so called ‘false positive’: electronic noise that resembles an image charge signal closely enough to be mistaken as a true ion detection event. In this case, an implantation is registered, although no ion is implanted. In contrast to this, in a post-detection method, the false positive and the false negative error rate have to be reduced at the same time, which generally demands higher SNRs and a detection efficiency close to 100% for a high fidelity of the implantation.

Studying the detection of ion bunches as a model for single ions of a specific charge state, we address the central question of this study: what is the relation of detection probability and the probability of false positive errors in dependence on the SNR? To investigate this, we developed an experimental approach to quantify the statistical distributions of signal and noise. In this context, it is not the aim to demonstrate the highest possible detection sensitivity. The presented results are relevant for the development of deterministic ion implantation methods, other applications of ICD and in general similar situations involving the statistical analysis of Fourier spectra.

2. Theory

The image charge detector employed in this study has five equally spaced, identical signal electrodes connected to the pre-amplifier input (see *experimental methods* below and [8]). When a charge with velocity v_{ion} passes through, this results in five successive peaks in the time domain output signal, according to the Shockley–Ramo theorem [3, 4, 8]. This can be viewed as a periodic signal with frequency $f_{\text{signal}} = v_{\text{ion}}/L_e$, where L_e is the distance between electrode centres (see also supplementary material (stacks.iop.org/JPhysD/52/305103/mmedia)). Performing a fast Fourier transform (FFT) on this signal gives a peak at f_{signal} with a certain FFT amplitude.

A Gaussian noise distribution in the time domain is transformed by an FFT to a probability density function (PDF) of the amplitudes described by the Rayleigh distribution [11, 12]:

$$\text{PDF}_R = \frac{1}{\sigma^2} x e^{-\frac{x^2}{2\sigma^2}}, \quad (1)$$

Table 1. Definition of true and false positive/negative in binary detection theory.

	Detection	No detection
Signal	True pos.	False neg.
No signal	False pos.	True neg.

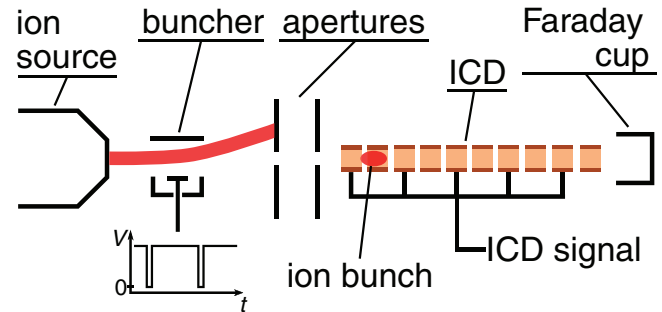


Figure 1. Schematic of the experimental setup for ICD. The ion beam (red) is interrupted periodically to produce ion bunches that are detected in the image charge detector (ICD).

with scaling parameter σ . A generalised form of the Gamma distribution can be used to model statistical noise with or without a signal contribution at a given frequency:

$$\text{PDF}_\gamma = \frac{2}{\beta^{2\alpha}\Gamma(\alpha)} x^{2\alpha-1} e^{-\left(\frac{x}{\beta}\right)^2}. \quad (2)$$

The scaling parameter β corresponds to the width of the distribution, which is related to the standard deviation of the Gaussian noise in the time domain. We found that the shape parameter α depends on the non-statistical signal contribution. For pure statistical noise, $\alpha = 1$ and with $\beta = \sqrt{2}\sigma$, PDF_γ reduces to PDF_R (equation (1)).

We define the SNR at the frequency f as

$$\text{SNR} = \frac{a_f}{n_{\text{rms}}}, \quad (3)$$

where a_f is the signal FFT amplitude and n_{rms} is the rms noise level at the signal frequency. A single measurement is counted as a detection, if the measured FFT amplitude v_f surpasses a specified detection threshold d . If a signal from an ion bunch is present and $v_f > d$, this is called a true positive (TP). The probability for a TP is found by integrating the PDF of the signal plus noise s_f above the threshold:

$$P_{\text{TP}} = \int_d^\infty s_f dv_f. \quad (4)$$

If a measurement contains only noise, the PDF is n_f and the probability to nevertheless count it as a detection (this is called false positive or FP) is given by

$$P_{\text{FP}} = \int_d^\infty n_f dv_f. \quad (5)$$

The common categories of detection or error types are summarised in table 1.

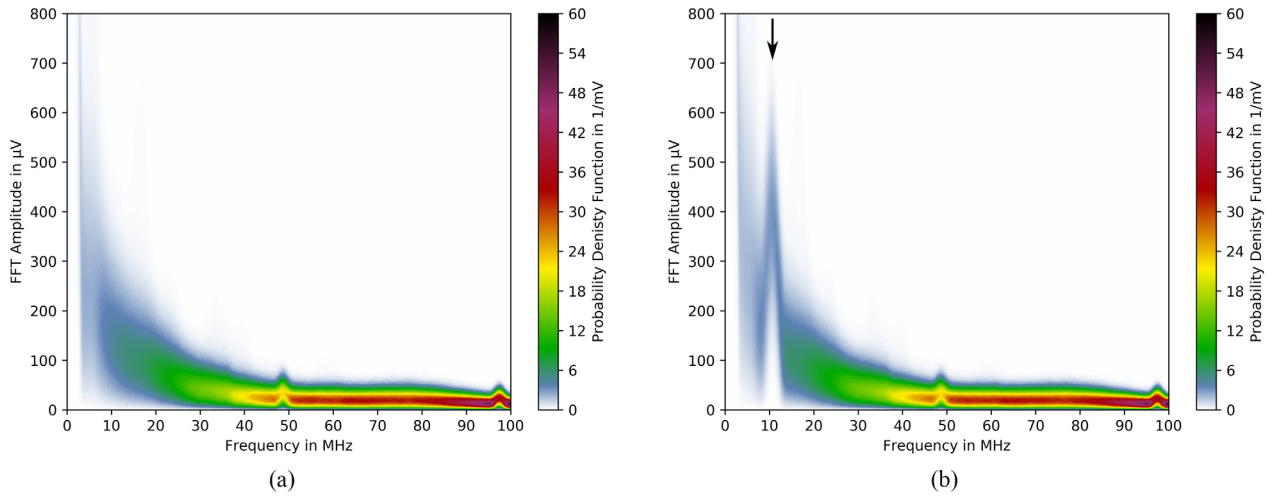


Figure 2. Probability density function of the FFT amplitudes at all frequencies up to 100 MHz, (a) noise, (b) with 10 keV Ar^{2+} ion bunch signal at $f = 10.55$ MHz (arrow) and 13.5 nA continuous beam current, i.e. $\text{SNR} = 2$.

3. Experimental methods

In the experimental setup (see figure 1) inside a vacuum chamber, the ion beam from an ion source with Wien filter is directed through the image charge detector (‘ICD2.5’). The base pressure in the chamber is approximately 1×10^{-6} mbar. The continuous beam current is measured with a Faraday cup behind the ICD. Short ion bunches are produced by interrupting the continuous ion beam by fast switching of a transverse electric field (buncher). The setup is described in more detail in [8]. In this study, Ar^{2+} and N_2^+ ions were used with accelerating voltages of 5 kV. The image charge detector is connected to the A250CF pre-amplifier [13] outside the vacuum chamber. A Rohde & Schwarz RTO2024 oscilloscope is used to perform FFTs of the pre-amplifier output signals and store the FFT spectra of all measurements for later analysis. The length of the waveforms was 1.1 μs .

4. Results

4.1. Noise and signal spectrum histograms

A large number of single measurements (6×10^4) have been recorded to obtain the PDF of FFT amplitudes over the whole spectrum (from 0–100 MHz). For each measurement the FFT was acquired and for every frequency (1230 bins), a normalised histogram of the measured FFT amplitudes was extracted. To measure this for the noise spectrum alone, the measurements were taken with the ion beam switched off (see figure 2(a)). The same procedure was then repeated with one ion bunch contributing to each single measurement to obtain s_f . The number of ions per bunch was determined from the continuous beam current, which was measured before and after every set of measurements to ensure beam stability. A typical result from an Ar^{2+} ion bunch signal with $\text{SNR} = 2$ at 10.55 MHz is shown in figure 2. The background spectrum remains unchanged far away from the signal frequency, while around the signal frequency the PDF shifts to higher FFT amplitudes.

The background noise consists mostly of statistical $1/f$ -noise up to 40 MHz and white noise. Above 80 MHz, the gain of the pre-amplifier decreases significantly. Minor non-statistical contributions are present at 47 MHz and 94 MHz. These interferences are caused by the Keithley 6485 Picoammeter used in the setup to measure the beam current and do not influence the spectrum at the signal frequency. The fast switching of the buncher has caused considerable interferences in the pre-amplifier circuit in earlier iterations of this setup [8]. Through optimised shielding and a larger distance of the buncher to the ICD, these interferences are reduced, so that the spectral PDF is the same with and without the switching of the buncher, except for very low frequencies that are irrelevant for the signals around 10 MHz.

4.2. Detection and error rates

To extract the noise PDF n_f at the signal frequency of 10.55 MHz, we consider the measured histogram at that frequency. It is shown in figure 3(a) with the red line representing a fit with the generalised gamma distribution (equation (2)). In this fit, $\alpha = 0.99 \approx 1$, which means that there is no significant non-statistical noise contribution. The rms-value is $n_{\text{rms}} = 191 \mu\text{V}$.

The data represented by the green fit curve in figure 3(a) shows the histogram at 10.55 MHz of the same signal as in figure 2. The fit with equation (2) is used to determine the maximum, which is $1.96 \cdot n_{\text{rms}}$, so that $\text{SNR} \approx 2$ (see equation (3)). The same measurement was repeated with various different numbers of charges per bunch by choice of different continuous beam currents. For each measurement, the beam current was adjusted and the buncher switched on to record 6×10^4 acquisitions. This took about 4 min and the beam current was checked again after completion of the measurement to ensure stability. All histograms measured with Ar^{2+} ion bunches are depicted with the fitted PDFs in figure 4(a). The maxima from the fits are extracted and shown in figure 4(b) as a function of the continuous beam current. The value at 0 nA is the maximum of the noise histogram. Above $\text{SNR} = 1$, there is a direct proportionality of the signal FFT amplitude on the

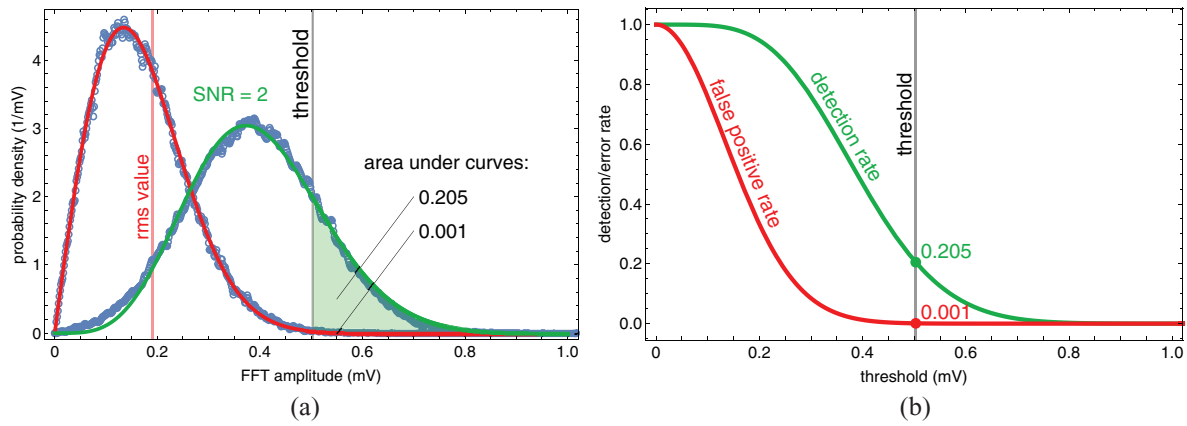


Figure 3. (a) Measured and fitted probability density functions for noise and Ar^{2+} signal with $\text{SNR} = 2$. (b) Integrated PDFs give the detection and false positive error rates.

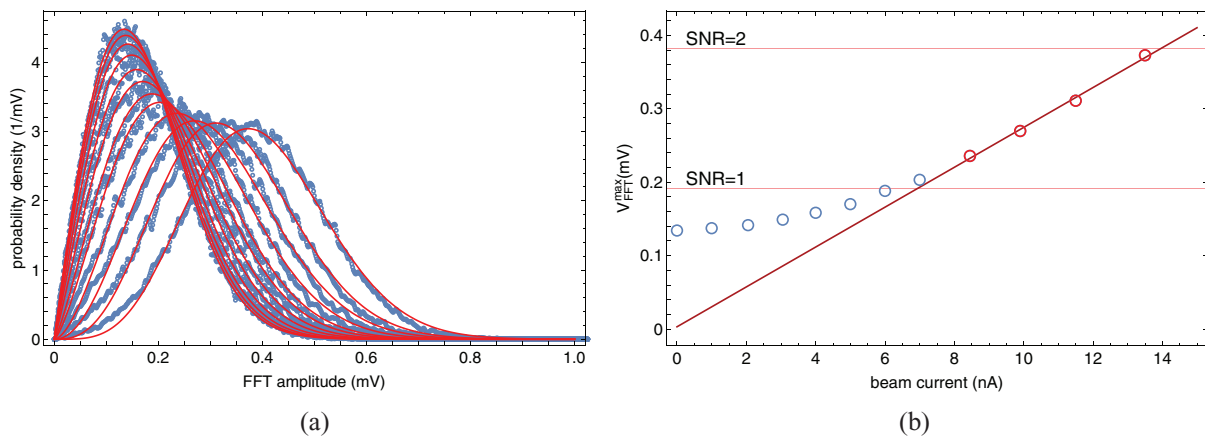


Figure 4. (a) Data and fitted probability density functions of all measured Ar^{2+} ion bunch signals and background noise at the signal frequency. (b) Maxima of the measured probability density functions of noise ($I_{\text{beam}} = 0$) and ion bunch signals. The red data points are used for the linear fit.

beam current, which is proportional to the number of ions per bunch. This is verified by the linear fit (red line) through the corresponding data points, which intersects the origin. Below $\text{SNR} = 1$, the maximum of the signal PDF asymptotically approaches the maximum of the noise PDF as the number of ions per bunch decreases.

The probability of a false positive and a TP detection can directly be deduced from this data. Figure 3(b) shows the integrals of the curves in figure 3(a) as a function of the detection threshold (see equations (4) and (5)). For example, if the threshold is set for a false positive rate (or probability) of 0.1%, the TP detection rate is 20.5%.

The same measurements were also performed with 5 keV N_2^+ ion bunches. The signal frequency here was 9.0 MHz. The noise at that frequency was slightly higher, with a value of $n_{\text{rms}} = 209 \mu\text{V}$. Similar to the analysis above, at $\text{SNR} = 2$, the detection rate was $P_{\text{TP}} = 22.8\%$ for a false positive rate of $P_{\text{FP}} = 0.1\%$.

In several different applications of binary detection theory, it is common to plot the TP rate as a function of the false positive rate. The resulting graph is called ‘receiver operating characteristic’ or ‘ROC curve’ [14]. The ROC curves of the Ar^{2+} ion bunch signals (see figure 4(a)) are shown in figure 5. A straight line from (0,0) to (1,1) corresponds to randomly

guessing, instead of detecting signals, i.e. a complete overlap of noise and signal PDFs. The inset graph in figure 5 shows a zoom of the values below 0.005, with the point (0.001, 0.205) marked, which corresponds to the threshold in figure 3(b).

To be able to estimate the number of ions per bunch, the ICD output voltage was calibrated against the continuous beam current as described in [8] (see also supplementary material). The Ar^{2+} ion bunch signal, that yields $\text{SNR} = 2$ in the FFT analysis corresponds to about 1100 ions per bunch, whereas for N_2^+ this number was 2200 ions per bunch.

From the analysis of the noise spectra (figure 2(a)), it seems advantageous to choose signal frequencies above 40 MHz for a lower rms noise value. This would imply a higher SNR for the same signal FFT amplitude, or a lower detection limit. However, for the same detector geometry, a higher signal frequency can only be achieved by a higher ion velocity. This has two disadvantages: on the one hand, the signal would be of shorter duration for the same detector length, the signal bandwidth would be higher, and so the FFT amplitude would be smaller in relation to the noise. On the other hand, higher kinetic energies above 10 keV are typically not interesting for high-precision deterministic ion implantation. Consequently, to access higher signal frequencies, the detector geometry has to be changed such that the signal electrodes are shorter and

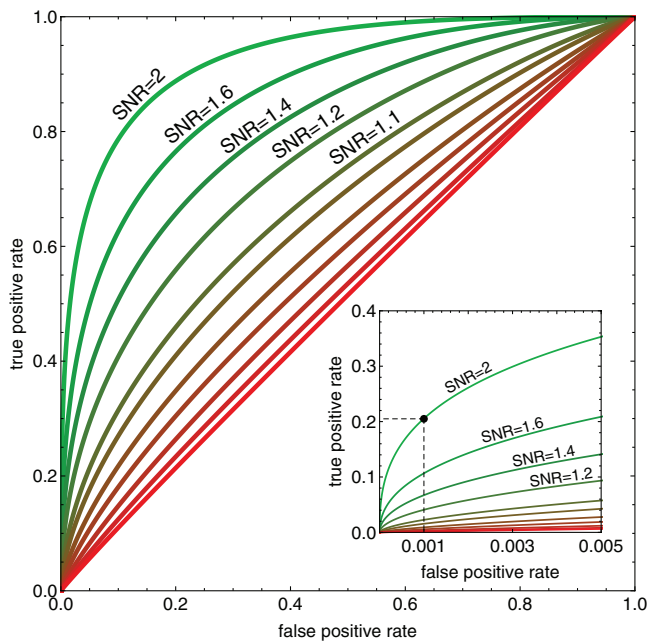


Figure 5. Complete ROC curves for the fitted Ar^{2+} ion bunch signals (same data as in figure 4(a)). Inset: detail of the ROC curves for low false positive rates, point marked for $\text{SNR} = 2$ and a false positive rate of 0.1%.

more closely spaced. However, this will change the signal form and noise characteristics, due to e.g. changes in the input capacitance, making a re-assessment of the noise spectrum necessary.

5. Conclusion

The noise spectrum and the signal properties of an ICD system were investigated. The presented measurement procedure is useful for determining different spectral contributions to the noise background over a great spectral range. It is possible to distinguish between statistical and systematic noise contributions. At the same time, the detection and error rates of single ion bunches with signals located at specific frequencies can be determined.

It was shown that the PDF of the FFT noise amplitude at the signal frequencies can be modelled by the Rayleigh distribution, because it is dominated by random statistical noise. Thus, the false positive error rate per measurement can be calculated as a function of the detection threshold for a given rms noise value. The TP detection rate depends on the SNR and on the false positive rate that is allowed. For example, at $\text{SNR} = 2$, the TP detection rate can be expected to be approximately 22%, when the threshold is set for a false positive error rate of $\approx 0.1\%$. From the theoretical considerations building upon the Shockley–Ramo theorem, this result can be expected to be independent from the ion species and the specifics of the experimental setup. From this, it can be concluded that $\text{SNR} = 2$ would be sufficient for most applications of deterministic ion implantation, using this pre-detection approach. For comparison, any post-detection method would have to exhibit the same false positive error rate (0.1%) and at the same time have a detection efficiency of 99.9% for a false

negative error rate of 0.1%, i.e. a comparable performance. This is a challenging demand, especially because post-detection methods rely on very specific sample properties, for example, high secondary electron yield or efficient charge collection for IBIC. For example, for IBIC detection, a 98% confidence is mentioned for an SNR of 6 for a 14 keV phosphorous implantation into silicon [15].

For future optimised detector setups the presented measurements are an effective test to probe for external noise sources and estimate detection and error rates for a given signal strength. Optimising the detector geometry, the electronic pre-amplifier circuitry and the signal analysis techniques, there is a huge potential to improve the detection sensitivity, which, however, was not the focus of this study, but of future work.

Acknowledgments

The authors would like to thank Roger John (Universitat Leipzig) for useful hints regarding data analysis. This work is carried out within the Leibniz Joint Lab ‘Single Ion Implantation’, and funded by the Leibniz Association (SAW-2015-IOM-1), the European Union together with the Sachsisches Ministerium fur Wissenschaft und Kunst (Project No. 100308873), the Volkswagen Stiftung and the German Academic Exchange Service (DAAD).

ORCID iDs

Paul Racke <https://orcid.org/0000-0002-1229-788X>

References

- [1] Keifer D Z, Pierson E E and Jarrold M F 2017 *Analyst* **142** 1654–71
- [2] Sugai T 2017 *Mass Spectrom.* **6** S0074
- [3] Shockley W 1938 *J. Appl. Phys.* **9** 635–6
- [4] Ramo S 1939 *Proc. IRE* **27** 584–5
- [5] van Donkelaar J et al 2015 *J. Phys.: Condens. Matter* **27** 154204
- [6] Jamieson D N, Lawrie W I, Robson S G, Jakob A M, Johnson B C and McCallum J C 2017 *Mater. Sci. Semicond. Process.* **62** 23–30
- [7] Tosi G, Mohiyaddin F A, Schmitt V, Tenberg S, Rahman R, Klimeck G and Morello A 2017 *Nat. Commun.* **8** 450
- [8] Racke P, Spemann D, Gerlach J W, Rauschenbach B and Meijer J 2018 *Sci. Rep.* **8** 9781
- [9] Meijer J et al 2006 *Appl. Phys. A* **83** 321–7
- [10] Matsukawa T, Fukai T, Suzuki S, Hara K, Koh M and Ohdomari I 1997 *Appl. Surf. Sci.* **117** 677–83
- [11] Rayleigh 1905 *Nature* **72** 318
- [12] Papoulis A and Pillai S U 2002 *Probability, Random Variables and Stochastic Processes* 4th edn (Boston, MA: McGraw-Hill)
- [13] Amptek 2017 A250CF specifications Amptek, Inc. (<http://amptek.com/products/a250cf-coolfet-charge-sensitive-preamplifier>)
- [14] Fawcett T 2006 *Pattern Recognit. Lett.* **27** 861–74
- [15] Jamieson D N, Lawrie W I L, Hudson F E, Dzurak A S, Morello A, Robson S G, Jakob A M, Johnson B C and McCallum J C 2016 *21st Int. Conf. on Ion Implantation Technology* pp 1–6